HiSST: 2nd International Conference on
High-Speed Vehicle Science Technology
11–15 September 2022, Bruges, Belgium

6DoF Aerodynamic Measurements of an Air-Breathing Hypersonic Vehicle

Patrick Gruhn[1], Sergej Blem[2], Ali Gülhan[3], Tobias Langener[4], Johan Steelant[4]
German Aerospace Centre (DLR), 51147 Cologne, Germany

Abstract

Aerodynamic stability is very important for high-speed aircraft configurations, where reaction times to disturbances can become quite short. Six-degree-of freedom measurements have been performed with a wind tunnel model of an air-breathing hypersonic vehicle. Mach numbers ranged between Mach 3.5 and Mach 8, utilizing two different wind tunnels. The angle of attack was varied between α = -3° and α = 3°, and the sideslip angle between β = 0° and β = 2°. Further on, the modular design of the model allowed for examining the influence of control surface deflections by canards, rudders and ailerons. Additional numerical calculations have been performed for certain test points. The tests gave insight into the aerodynamic properties of the configuration and helped to determine flight conditions with critical or unstable longitudinal and lateral stability, respectively. Further on, the influence on the aerodynamics of the vehicles that is caused by changes in the flow state at the engine intake was shown.

Keywords: *6DoF measurements, Scramjet, Aerodynamic stability*

Nomenclature

Latin
A – Area [m²]
C – Aerodynamic coefficient
M – Mach number
Re – Reynolds number
T – Temperature [K]
l – Length [m]
p – Pressure [Pa]
s – Span width [m]
u – Velocity [m·s^{-1}]

Greek
α – Angle of attack [deg]
β – Sideslip angle [deg]
δ – deflection angle [deg]
ρ – Density [kg·10^{-3}]

Subscripts
∞ – Ambient condition
D – Drag
a, c, r – Aileron, Canard, Rudder
ref – reference value or condition
t – total flow condition

1. Introduction

Different concepts for high-speed civil aircraft have been suggested in recent years [1-3]. It was shown that the correct determination of the aerodynamic and propulsive performance of the vehicle is crucial

[1] *Research Scientist, Supersonic and Hypersonic Technologies Department, Institute of Aerodynamics and Flow Technology, Linder Höhe, 51147 Cologne, Germany, e-mail: Patrick.gruhn@dlr.de*
[2] *Research Scientist, Supersonic and Hypersonic Technologies Department, Institute of Aerodynamics and Flow Technology, Linder Höhe, 51147 Cologne, Germany*
[3] *Department Head, Supersonic and Hypersonic Technologies Department, Institute of Aerodynamics and Flow Technology, Linder Höhe, 51147 Cologne, Germany*
[4] *Senior Engineer, ESA-ESTEC, Flight Vehicle and Aerothermodynamics Engineering Section TEC-MPA, P.O. Box 299, Noordwijk, Netherlands, Tobias.Langener@esa.int, Johan.Steelant@esa.int,*

for assessing the concepts feasibility. This becomes even more true for hypersonic aircraft equipped with air-breathing engines, where small variations can lead to large errors in trajectory calculations [4]. On top of that, aerodynamic stability can become sensitive to changes in flight conditions [5], but has to be maintained at all conditions. Because of the highly integrated design, the flow field around such vehicles is normally quite complex and features strong flow interactions, thus making it challenging to predict the aerodynamic performance with common engineering design tools [6]. Reliable predictions ahead of flight tests are currently either achieved by sophisticated nose-to-tail CFD simulations or by dedicated wind tunnel experiments.

This manuscript presents two experimental test campaigns that were performed in order to determine the aerodynamic properties of the scaled down LAPCAT-II Mach 8 vehicle [7] in the supersonic and hypersonic flight regime. The objective of the tests was to determine the aerodynamic performance of the vehicle in order to support the design and to provide input data for the aerodynamic control of the vehicle. In preparation towards these experiments, a dedicated CFD campaign was performed to provide the forces and moments expected for the balance. Mutually, the tests provided also an experimental data base for the verification of CFD codes and for the assessment of the full-scale vehicle's aerodynamic performance.

2. Setup

2.1. Wind tunnels

The wind tunnel model was tested in two blow-down type wind tunnels of DLR in Cologne. Test at two supersonic Mach numbers (M_∞ = 3.5 and M_∞ = 4.0) were performed in the Trisonic Test Section (TMK). It has a square test section of 600mm x 600mm. It has an adjustable contoured nozzle that allow for changing the Mach number during a test run. The typical duration of a test is between 30 and 60 seconds. Test at hypersonic Mach numbers (M>5) were performed in the hypersonic test section H2K. It uses different contoured Laval nozzle of 600mm diameter for different Mach numbers. In the range between M_∞ = 5.3 and M_∞ = 11.2. The flow is heated up by an electrical heating system with 5MW of power in order to vary flow conditions and to avoid flow condensation during expansion in the nozzle. Depending on the flow conditions tests times up to 30s can be achieved. The operating range of both wind tunnels is given in Fig 1 as Mach Reynolds diagram. Marked dots in the diagrams indicate the nominal flow conditions for the presented wind tunnel tests. They are also given in Table 1.

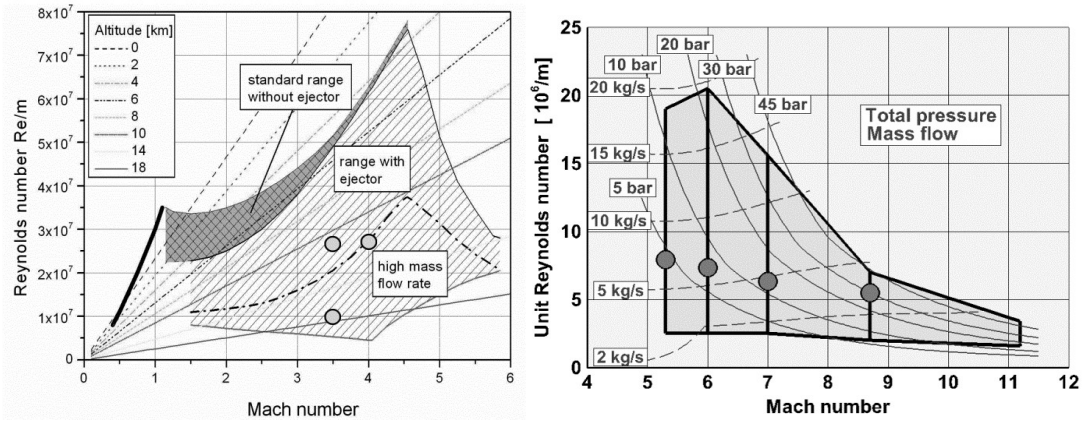

Fig 1. Operating range of Trisonic Test Section TMK (left) and Hypersonic Test Section H2K (right).

Table 1: Nominal test conditions

Cond.	M_∞	Re, m^{-1}	p_t, Pa	T_t, K
I	5.306	$7.9 \cdot 10^6$	730,000	500
II	6.027	$7.3 \cdot 10^6$	912,000	500
III	7.049	$6.3 \cdot 10^6$	1,314,000	540
IV	8.778	$5.5 \cdot 10^6$	3,300,000	730
V	3.5	$10.9 \cdot 10^6$	182,000	290
VI	3.5	$26.7 \cdot 10^6$	445,000	290
VII	4.0	$27.6 \cdot 10^6$	582,000	285

In Fig 2, the test conditions are given in comparison to the flight trajectory of the LAPCAT 2 vehicle. The top diagram shows the flight trajectory of the full-scale vehicle as result of the trajectory optimization performed in [8]. The bottom diagram shows the Mach-Reynolds diagram for the same trajectory, now adapted for the LAPCAT II mall-scale-test vehicle. Test condition I to III closely match the trajectory. Test conditions IV was chosen as high-speed case, and as no Mach 8 nozzle was available at that time. Test condition V has a slightly lower Re value, because the original similarity analysis was performed on a preliminary reference trajectory, that featured slightly higher altitudes at Mach numbers below 4 than the final optimized trajectory. Finally, test conditions VI and VII were chosen as high Reynolds test cases in order to force early transition of the boundary layer on the inlets surfaces. Therefore, the boundary layer was artificially tripped for most of the tests at these conditionsby applying 400µm carborundum particles in a 10mm wide strip, starting 15mm downstream of the leading edge of the model.

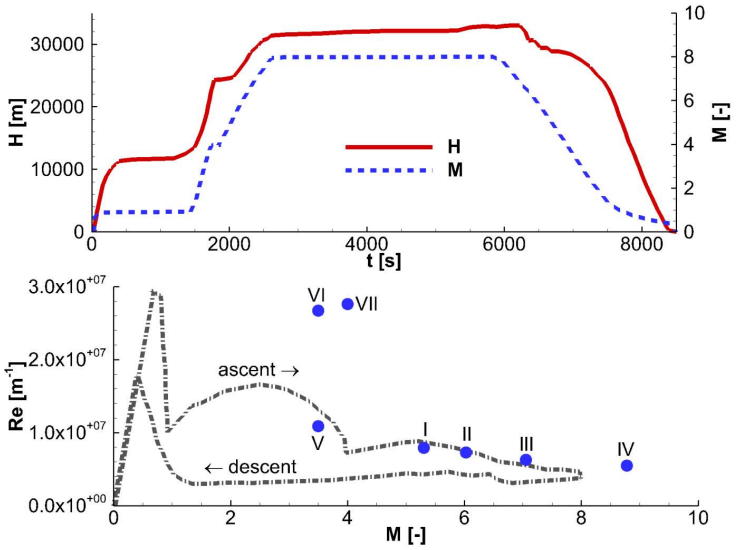

Fig 2. Flight Mach number and altitude vs. mission time [8]; Bottom: Derived Mach-Reynolds diagram for small scale vehicle trajectory and test conditions.

2.2. Wind tunnel model

The wind tunnel model used for the tests is a 1:2 scale representation of the LAPCAT II small scale Mach 8 vehicle. It is shown in Fig 3. It has an overall length of l = 720mm and a max. span width of s ≈ 342mm. The model is made of titanium, and is equipped with two internal ducts representing the engine flow paths of the ATR- and the scramjet engine. For tests at supersonic Mach numbers, i.e. tests in the TMK, both flow ducts were open. For the hypersonic tests in the H2K, the ATR flow duct was closed by a removable lid, so that only the scramjet flow duct was open. This emulates the "sliding door" concept foreseen for the flight vehicle, where the ATR duct (designed based on the XB-70 air induction system [9]) is also closed during cruise flight. For measuring aerodynamic forces and moments, the model was equipped with two different internal Six-degree-of-freedom (6DoF) strain gauge balances, whose measuring range closely matched the expected loads.

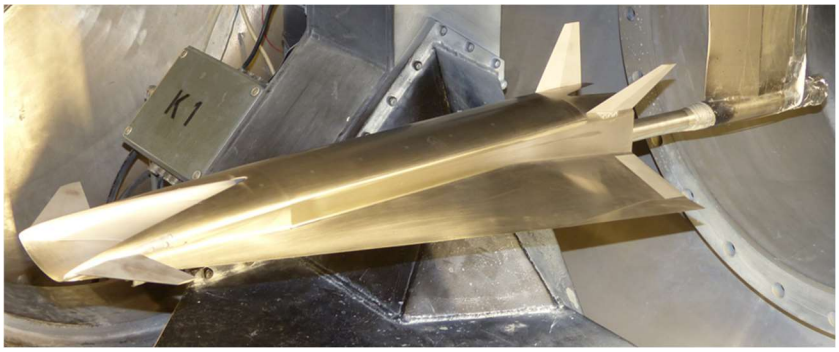

Fig 3. Wind tunnel model in H2K test section

In order to study the aerodynamic behavior at different aerodynamic settings, the wind tunnel model is equipped with exchangeable control surfaces for canards, rudders and ailerons. The canard deflection angle can be varied between δ_c = -2° and δ_c = +6° (here, a positive deflection angle is defined as one that creates lift and a pitch-up moment). Another blind set is available to test the vehicle without canards at all. Five aileron inserts for each wing enable to set aileron deflection angles of δ_a = -20°; δ_a = -15°; δ_a = -5°; δ_a = 0° and δ_a = +5° (again, a positive deflection is defined as one that creates lift (and a pitch-down moment in this case)). Finally, three rudder inserts per side are available, with deflection angles of δ_r = -5°; δ_r = 0° and δ_r = 5°. The rudder deflection angle is defined as positive when it causes a side force to the direction of the model side where the rudder is installed (i.e. a positive deflection of the left rudder causes a force to the left, and vice versa). For clarification, the coordinate system and the angle definitions used are shown in Fig 4.

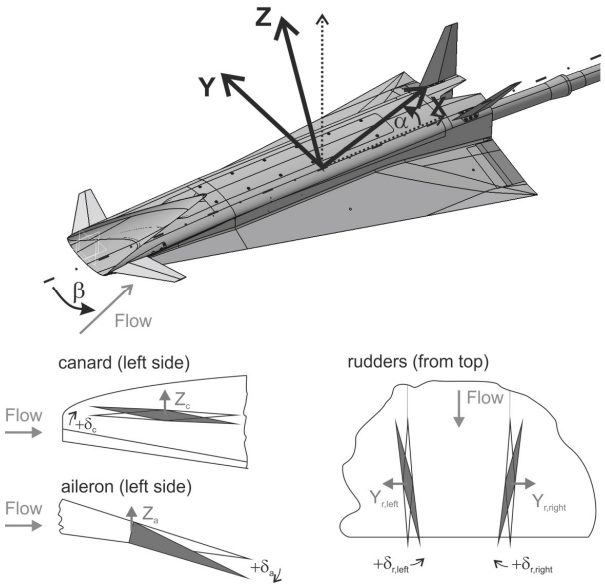

Fig 4. Definitions of coordinate system, angle of attack, sideslip and surface deflections.

3. Experimental results

Altogether, 85 wind tunnel tests were performed in the two test series. Thereby, each test series was split into three parts: the first on the aerodynamics of the reference configuration without surface deflections and at zero sideslip, the second on the influence of the side slip angle, and the third on the influence of control surface deflections. Fig 5 shows measured aerodynamic coefficients of axial force (top left), normal force (top right), pitching moment (bottom left) and lift-to-drag ratio (bottom right) for the reference configuration at hypersonic Mach numbers (H2K tests). As reference dimensions the model length l_{ref} = 0.72 and the projected frontal surface area A_{ref} = 0.0189m² are used. The moment center is located on the vehicle axis, at a relative position of x/l_{ref} = 58%.

While the results here are shown for the vehicle configuration without Canards (i.e. with "blind" inserts"), similar results were found for the configuration with Canards, with only minor differences due to the added effect of the Canards. Most interesting is the pitching moment which is negative throughout the test range, demonstrating a pitch-down tendency of the vehicle (at least for the given reference point and at engine-off conditions). Further on, the gradient of the pitching moment is positive, indicating a longitudinal unstable configuration. One further point of interest is the sudden jump in the curves for Mach numbers M_∞ = 7.0 and M_∞ = 8.7. These can be traced back to an 'unstart' of the intake flow of the vehicle, resulting in a sudden change of the flow field topology that was observable in the Schlieren videos of the test. Thereby, the observed flow fields matched those of dedicated intake tests in the same wind tunnel that had been performed as part of the same project [10]. The aerodynamic results here demonstrate that such unstarts have to be avoided because they cause sudden changes in the aerodynamics which cause disruptions of the flight and have to be caught by the control system (next to the loads and stresses that an unstart itself causes on the structure).

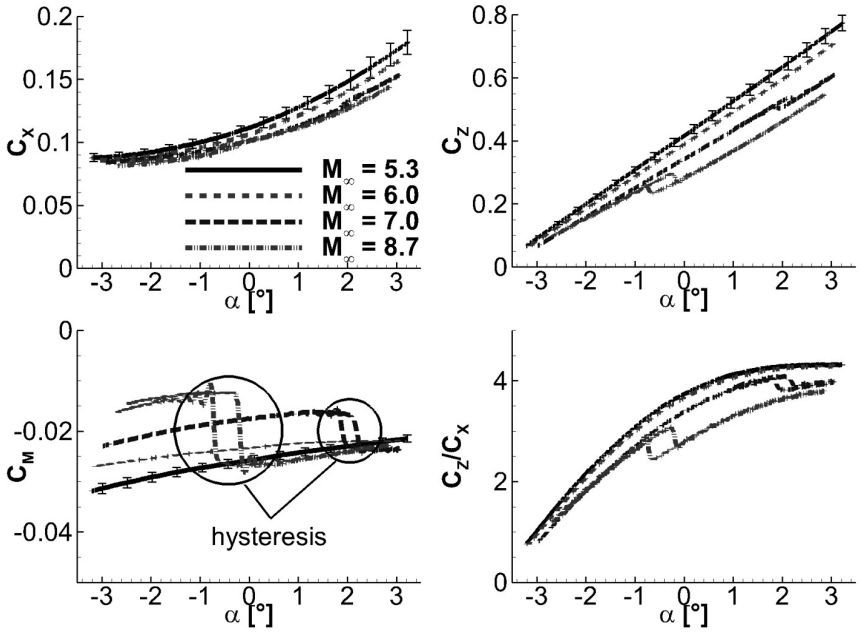

Fig 5. Coefficients of axial force (top left), normal force (top right), pitching moment (bottom left) and lift-to-drag ratio (bottom right) for reference configuration without Canards (H2K tests).

In Fig 6, the results for the reference configuration with (B) and without Canards (A) at supersonic Mach umbers (TMK tests) are shown. Again, only small differences are seen in the lift and drag coefficients for both configurations, with a slightly higher lift-to-drag ratio for the configuration without Canards. Also, like at hypersonic Mach numbers, the difference between the two configurations is much more prominent in the pitching moment, because the off-center canards have a strong influence here. Again, the pitching moment of the vehicle is negative throughout the angle of attack range, indicating the same pitch-down tendency of the vehicle at engine-off conditions as observed for hypersonic conditions.

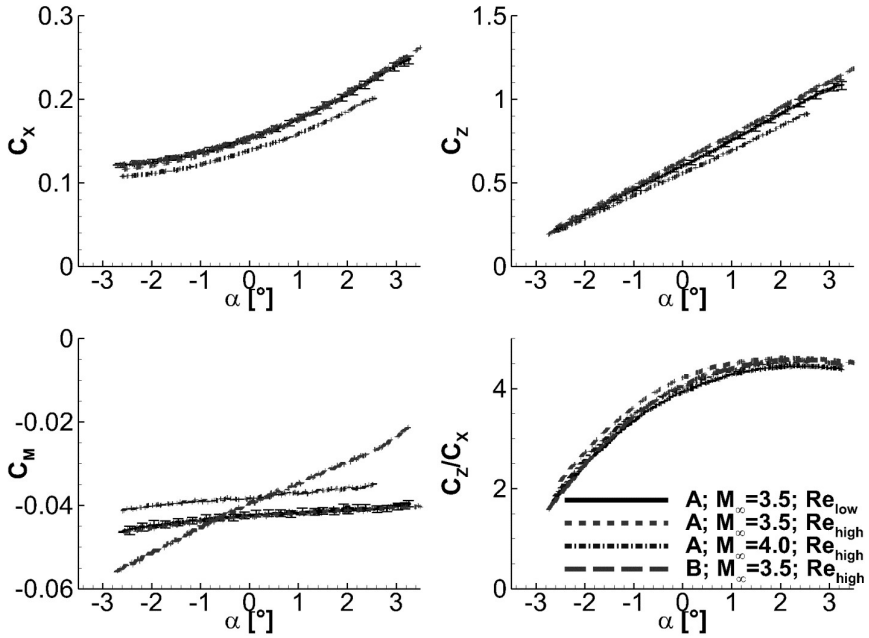

Fig 6. Lift, drag, pitching moment and lift-to-drag ratio for reference configuration without (A) and with canards (B) at zero sideslip.

Tests at sideslip conditions revealed a certain sensitivity of the intake with respect to the side slip conditions. In the H2K tests, the intake flow was unstarted throughout the test at Mach 5.3 and Mach 6 for a sideslip angle of $\beta = 2°$. Only at $\beta = 1°$ a started inlet was observed. At Mach 7, a started inlet was observed for $\beta = 2°$, but the inlet subsequently unstarted during the test at an angle of attack of

α ≈ 2.4°. On the downward branch of the α-sequence, the inlet restart occurring at α ≈ -1.1°, leading to a prolounged hysteresis in the curves (see Fig 7).

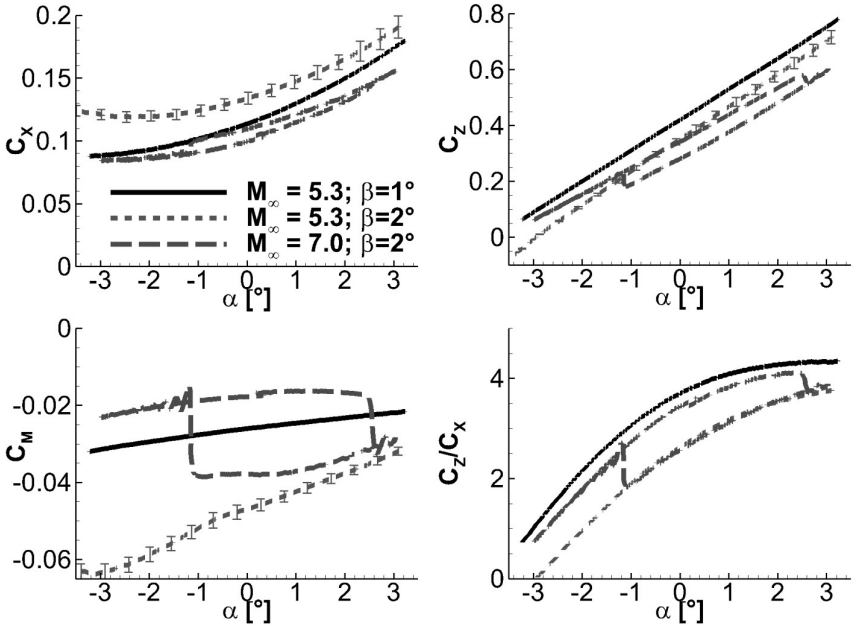

Fig 7. Lift, drag and pitching moment for reference configuration without canards at sideslip.

In Fig 8, the aerodynamic coefficients of side force, yawing moment and rolling moment for the same test cases are shown. As can be seen, absolute values of side force and yawing moment are higher for started inlet conditions, probably due to the added compression on the leeward side of the inlet. The yawing moment is found negative throughout the test range, implying a lateral unstable vehicle, at least for the chosen point of reference chosen. A small rolling moment (with roll stability only for positive angles of attack) is induced by the dissimilar flow on both sides of the vehicle. Comparing the curves for M_∞ = 5.3 shows that the rolling moment is smaller at β=2°, meaning that at least for the conditions investigated here the gradient of $C_{L\beta}$ is negative, implying "dihedral effect stability" (i.e., in case of a sideslip disturbance, the vehicle would roll away from the disturbance decreasing sideslip).

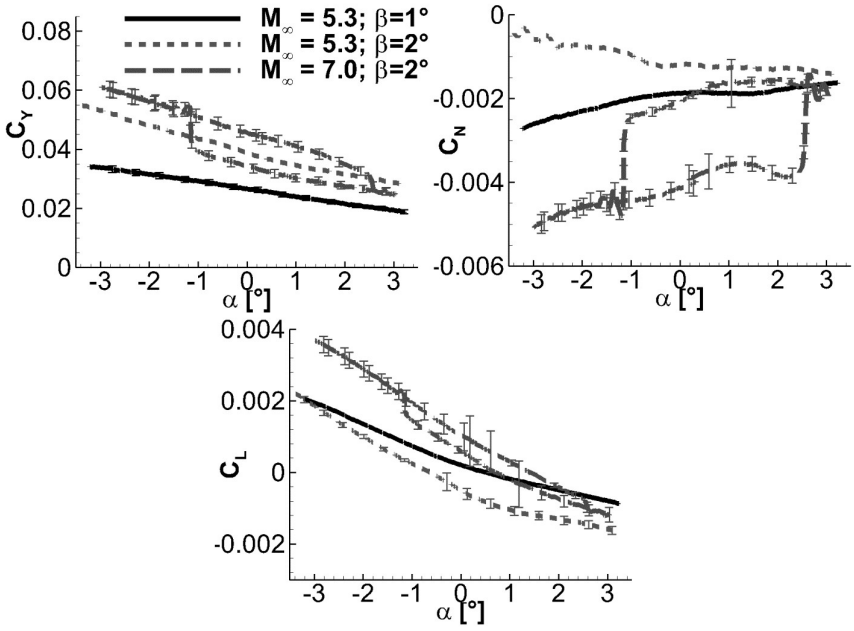

Fig 8. Side force, yawing and rolling moment for configuration without canards at sideslip

The same lateral instability was observed at Mach 3.5 and Mach 5 (TMK tests, not shown here). Though no full unstart was observed in these test cases with both flow ducts open, there were some notable

oscillations of the side force and the yawing moment, with a frequency of about 10-11 Hz. Though not fully conclusive, the most probable cause for this is a partial blockage of one of the two internal ducts, leading to some transient behavior at the inlet (kind of "buzzing"). Such a partial blockage was found in the CFD calculations by ESA at a slightly lower Mach number of M_∞ = 3.25. In support of this assumption, some oscillations of the shock system just above the inlet have been observed in the high speed Schlieren recordings.

Finally, the results of different setups to create either pitch-up or pitch down moments are shown in Fig 9, for the case of Mach 5.3. Similar results were found for the other Mach numbers. Either only canards or aileron have been deflected, or both, in order to create the maximum pitch-down (upper diagrams) or pitch-up (bottom diagrams) effect. For comparison, the long-dashed line in the diagrams shows the neutral configuration. Naturally, the greatest effect on C_M is obtained when both sets of control surfaces responsible for pitch control are deflected (solid lines). The effect on C_M when deflecting only the canards (dotted lines) or only the ailerons (dashed lines) to their respective maximum deflection is about the same. However, in case of a "pitch-up" deflection, a difference is seen in the lift-to-drag ratio, due to the different direction of the normal forces created by the control surfaces. These differences are smaller for the "pitch-down" cases, because the overall deflection angles here are also smaller.

One important observation is, that for the "pitch-up" configuration (and only for the hypersonic test cases), negative values of C_M are found at angles of attack below $\alpha \approx -1°$, even for maximum surface deflection. This shows an unstability wtr to pitching and shows that the vehicle in its current configuration could not be be controlled if the angle of attack drops below $\alpha \approx -1°$ (at least for engine-off conditions). In order to regain stability, it was recommended to either increase the size of the control surfaces or to shift the moment reference point (i.e. center of gravity). Both of these recommendations have been implemented in the design of the vehicle investigated in the follow-on project HEXAFLY EU-FP7, see [11, 12]. These studies on the follow-on vehicle showed also showed a beneficial effect of engine on conditions on trimming and longitudinal stability of the vehicle [12], rendering the cases studied in the wind tunnel tests described here as "worst case" scenarios.

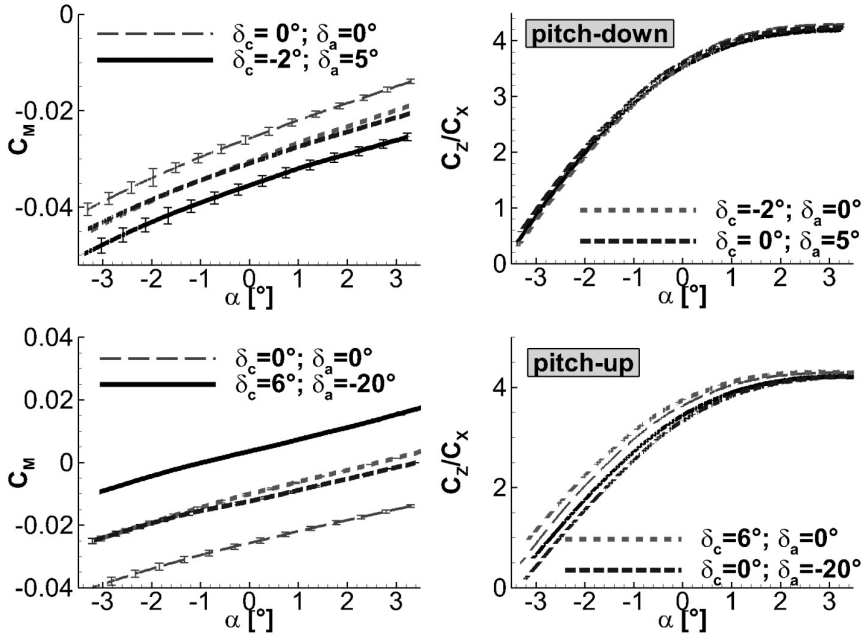

Fig 9. Pitching moment and lift-to-drag ratio for configurations with surface deflections intended for "pitch-down" (top) or "pitch-up" (bottom; both M_∞ = 5.3; β = 0°).

Regarding lateral stability, the effectiveness of the rudders was found to be sufficient for the lateral control of the vehicle, at least for the sideslip angles tested. The yawing moment (not shown here) was found positive throughout the test range in case of deflected rudders, which means that the sideslip angle can be reduced in flight, thus assuring static lateral stability (for the engine-off condition investigated here). However, since the nozzle is symmetric wrt the x-z plane, this should be true for

engine-on conditions as well. Also, the authority to control the rolling moment by simultaneous deflection of canards, aileron and rudders was found to be sufficient for all test cases.

4. Numerical Assessment

To support the design of the aerodynamic wind tunnel model, especially at low Mach numbers as tested in DLR's TMK wind tunnel, several CFD simulations using DLR's TAU code were carried out to determine where the intake unstarts and to have numerical data available to compare the experimental results against.

4.1. Numerical Modelling

For the nose-to-tail simulation of the aeromodel, ESTEC used the hybrid structured/unstructured DLR-Navier-Stokes solver TAU, which is validated for a wide range of steady and u =nsteady subsonic, transonic and hypersonic flow cases is used. The TAU code is a second order finite-volume flow solver for the Euler and Navier-Stokes equations in the integral form using eddy-viscosity, Reynolds-stress or detached- and large eddy simulation for turbulence modelling. The AUSMDV flux splitting scheme is applied together with MUSCL gradient reconstruction to achieve second order spatial accuracy.

For the present investigations, the Spalart-Allmaras one-equation eddy viscosity model is used for the viscous simulations. Also, inviscid simulations are carried out which represent in a way the limit when the effects of boundary layer, e.g. displacement and separation, are annihilated as classically done on intakes by means of BL-suction.

The initial mesh for the nose-to-tail simulations had a size of approximately 5.3 million nodes. After several gradient based refinement steps to better resolve for example shock structures, this number grew to approximately 11 million mesh points. The simulations were always started on the unrefined mesh for all Mach numbers studied and then the mesh refinement loops were initiated due to the different flow topology at different Mach numbers.

The mesh was designed for the turbulent simulations (hybrid mesh resolving the boundary layer regions) but was also used for the inviscid calculation for simplicity reason and due to the fact that computational recourses were readily available.

To ensure starting of the intake in the simulation also at the higher Mach number, the flow field was initialized at M=4.5 for all cases. Stepwise the free-stream Mach number was reduced via shell scripts till the wanted Mach number. This methodology was exploited to assure the initial solution originated from a started configuration. Hysteresis effects were not addressed in the present study.

All walls were set to 300 K (constant wall temperature boundary condition). The following inflow conditions (Table 2) were used for at the farfield boundaries:

Table 2: Boundary Conditions

	ρ [kg/m³]	T [K]	M [-]	u [m/s]	p [Pa]	Re/m [1/m]
M=4.5	0.5965	133.33	4.500	1,041.6	22,825	6.75E+07
M=3.75	0.5965	133.33	3.750	868.0	22,825	5.62E+07
M=3.25	0.5965	133.33	3.250	752.2	22,825	4.87E+07
M=3	0.5965	133.33	3.000	694.4	22,825	4.50E+07
M=2.75	0.5965	133.33	2.750	636.5	22,825	4.12E+07
M=2.5 (TMK reference)	0.5965	133.33	2.500	578.6	22,825	3.75E+07
M=1.85	1.2299	178.09	1.850	494.9	62,862	5.07E+07
M=1.2	2.4058	232.92	1.200	367.1	160,822	5.85E+07
M = 0.9	3.1120	258.18	0.900	289.9	230,591	5.50E+07

One can see that for M=2.5 up to M=4.5 the same thermodynamic free stream state was assumed. The conditions for M=2.5 represent the conditions of DLR's TMK wind tunnel. For the inviscid

simulations the intake performance is evidently not dependent on the thermodynamic free stream properties, while it has for the viscous simulations.

4.2. Aerodynamic Performance

Fig 11 and Fig 13 give the outcome of inviscid computations for the complete aeromodel which include the control surfaces, i.e. canards, ailerons, rudders. The simulations were done for Mach 1.20, 1.85, 2.50, 2.75, 3.00, 3.25, 3.75 and 4.50 with the AoA set to zero. The lift coefficient is given in Fig 11 both for the external flow paths as for the overall one, i.e. including the internal flowpath. For trajectory analysis under propulsive power, the aerodynamic performances are defined by the external surfaces only whereas the internal flowpath is always considered as part of the propulsive database. In case of pure gliding, i.e. propulsion is off, the total overall values need to be used. One clearly notices that the lift performance is nearly completely defined by the external surfaces and that small effects are most likely coming from the intake spillage. The largest difference between total and external surfaces can be noted for the drag component which is purely due to the viscous drag stemming from the internal flowpath.

The aerodynamic performance is given in Fig 13 where the inviscid L/D is above 9 for all considered Mach numbers. For pure gliding with propulsion on, the L/D drops considerably to values around 4 for $M < 3.25$. The L/D jumps above 6 for $M > 3$ which is due to the start of both the low and high-speed duct (Fig 10) reducing considerably the spillage drag.

Fig 12 provides the aerodynamic coefficients C_D and C_L for turbulent viscous calculations. The C_L doesn't differ much from the previous inviscid calculations. The total and external C_D is obviously higher than the inviscid part. The lower the Mach number the larger the impact on the total drag coefficient is which is more than double than the external C_D at $M = 1.25$.

With respect to the external aerodynamic efficiency L/D, the viscous contribution drops the L/D to about 6, independently of the Mach number (Fig 14). The L/D defined purely on pressure (Fig 14) is not-surprisingly very close the inviscid values (Fig 13). For the total L/D, e.g. applicable for pure gliding, the values evolve from 4 at Mach 4 to around 3 for $M \approx 1$. Theoretically, this means that the vehicle will lose height quickly during the gliding descent. However, one should notice that the calculations were done for cold wall. This condition provides a large viscous contribution resulting into too low L/D compared to simulations with e.g. radiative equilibrium.

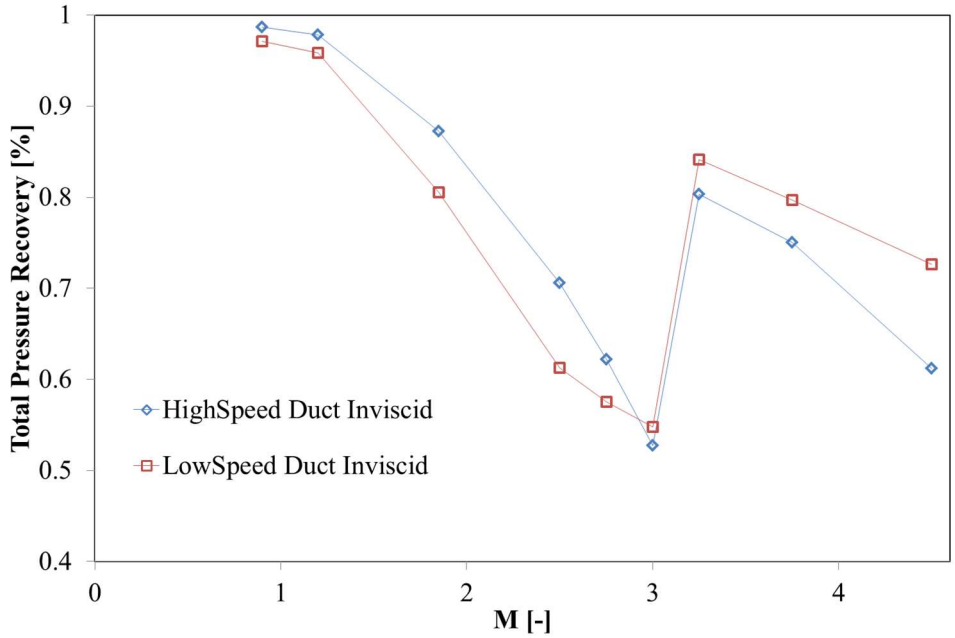

Fig 10. Total Pressure Recovery of the High-Speed duct and Low Speed duct from Inviscid Calculations.

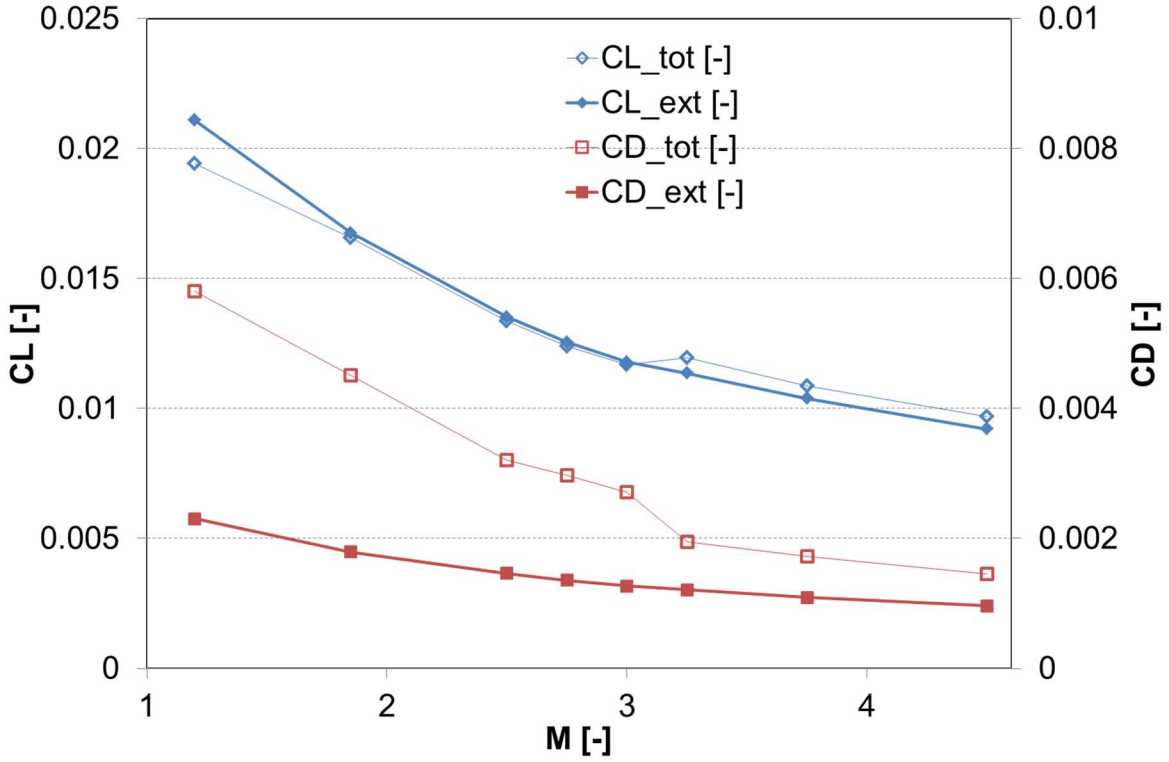

Fig 11. Aerodynamic coefficients of Lift and Drag from inviscid simulations: contribution of external flowpath only and the combination of both external and internal flowpath.

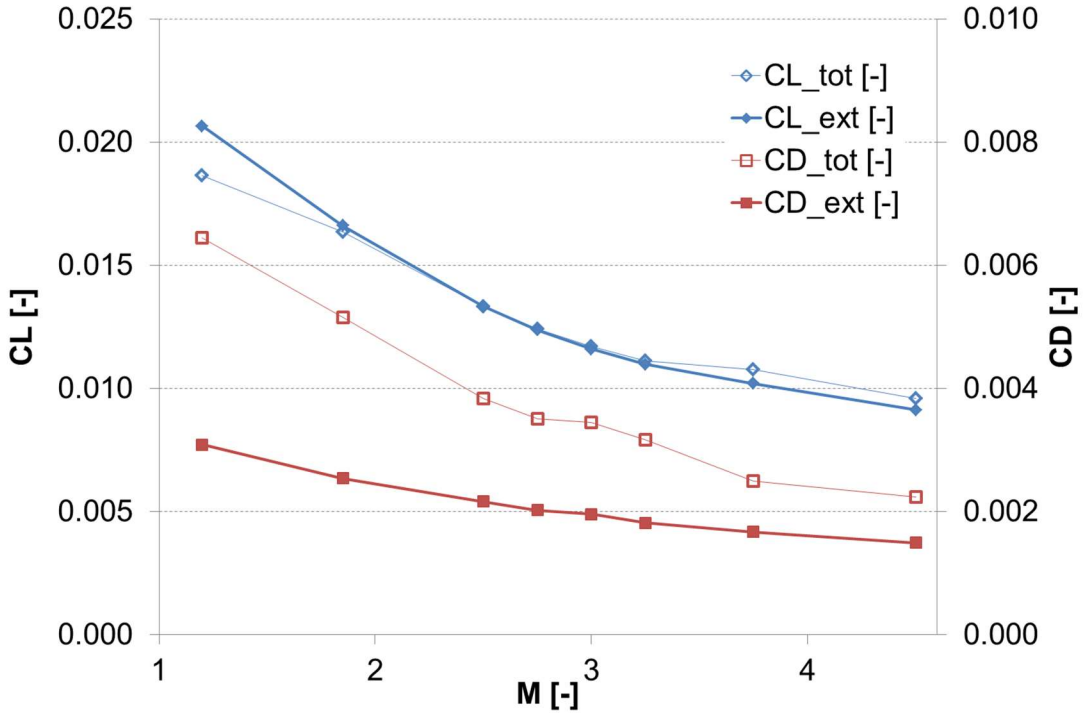

Fig 12. Aerodynamic coefficients of Lift and Drag from turbulent simulations (RANS): contribution of external flowpath only and the combination of both external and internal flowpath.

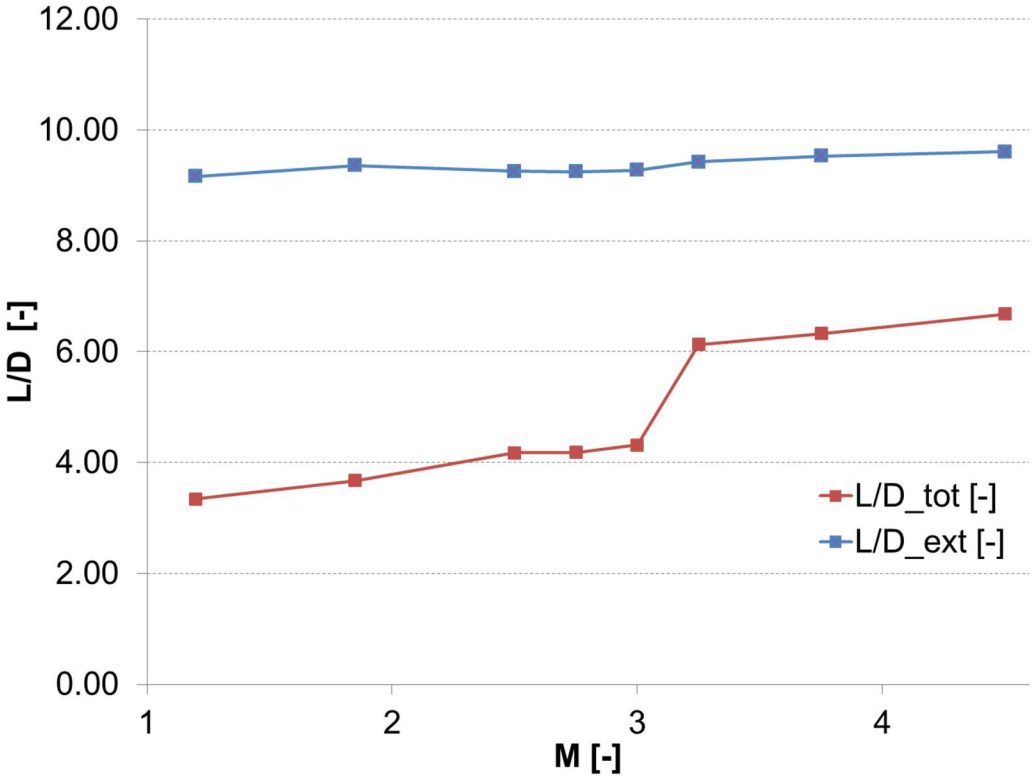

Fig 13. Aerodynamic efficiency from inviscid simulations: contribution of external flowpath only and the combination of both external and internal flowpath.

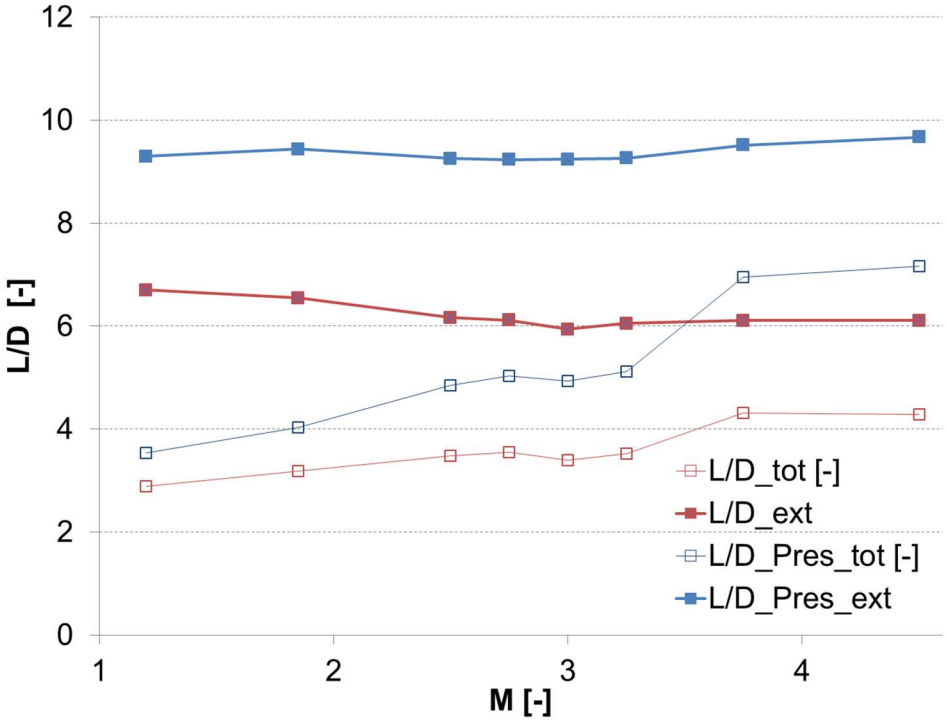

Fig 14. Aerodynamic efficiency from turbulent simulations (RANS): pressure (closed symbols) and full contribution (open symbols) of external flowpath only and the combination of both external and internal flowpath.

5. Conclusion

A model of a small-scale air-breathing hypersonic vehicle has been tested in the Trisonic Test Section (TMK) and the Hypersonic Test Section Cologne (H2K) of DLR in Cologne, at velocities ranging from high supersonic (Mach 3.5) to hypersonic speeds (up to Mach 8.7). Aerodynamic measurements have been performed with help of six-degree-of-freedom balances at various angles of attack, different sideslip angles, and for different vehicle configurations with various control surface deflections (canards, rudders and ailerons). Additionally, in order to support the design of the aerodynamic wind tunnel model and to have numerical data available to compare the experimental results against, several CFD simulations using DLR's TAU code were carried out to determine where the intake unstarts, especially at low Mach numbers as tested in DLR's TMK wind tunnel.

The aerodynamic measurements exhibited a strong pitch-down tendency of the vehicle in the tested configuration and for the given center of reference at engine-off conditions (which were subject of the tests). In the hypersonic range, the pitch-down moment could not be compensated by a deflection of the canard and ailerons, at angles of attack below $\alpha \approx -1°$, which means that the vehicle cannot be controlled if the angle of attack drops below this value. The pitch-down tendency was observed at supersonic Mach numbers, too, but here the control surfaces were found to be sufficient to trim the vehicle with respect to pitching motions. The vehicle was also found to be laterally unstable. However, the rudder effectiveness was found to be sufficient for stabilizing the vehicle. Also, induced rolling moments can be compensated by adequate settings of all control surfaces.

Another important aspect shown is the effect of changes of the engines (or more specifically, the inlets) state on the aerodynamics of the overall vehicle. In the hypersonic tests, with the ATR duct covered, the unstart of the inlet leads to an abrupt change of the aerodynamic characteristics, especially concerning the pitching moment, where the pitch-down tendency of the vehicle was increased. These changes were subject to some hysteresis with respect to the angle of attack where start of unstart of the inlet occurred, and this was especially strong at sideslip conditions. Further on, oscillations at supersonic Mach numbers indicated that the scramjet duct was partially unstarted and in a "buzzing" state. This shows that interactions between the two ducts have to be considered during design as well.

In summary, the experiments provided insight into the aerodynamic properties of the small-scale vehicle and gave valuable information for the further layout and design. It was recommended that the size of the canards and ailerons should be increased, and/or the center of gravity should be shifted in order to reduce the longitudinal and lateral instability of the vehicle. These recommendations have then indeed been implemented in the follow-on project. Further on, the sensitivity of the aerodynamics to the state of the inlet flow shows demonstrated that either the vehicle attitude has to be tightly controlled, in order to avoid off-design conditions and eventual unstarts of the inlet, or the robustness of the inlet and flight configuration overall against unstart has to be improved. Since the inlet unstart observed here were probably related to a large laminar separation at the first "kink" between the frontal area and the inlet ramp, artificial tripping of the boundary layer or simple scaling up of the vehicle might help in this regard. Finally, the experimental data was used for validation of nose-to-tail CFD computations of the vehicle, thus increasing confidence in numerical predictions of the full flight path.

References

1. Wall, R., Norris, G., "Filling a Gap – Interest rises in high-speed premium air-travel aircraft", Aviation Week & Space Technology, p.38, 27th June 2011.
2. Blanvillain, E., "A Holistic Approach To Hypersonic Aircraft Design: ZEHST (Zero Emission High Speed Technologies)," 29th Congress of the Aeronautical Sciences, St. Petersburg, Russia, Sept. 7-12 2014.
3. Steelant, J., "European Activities on High-Speed Vehicles: Feasibility Studies and Technological Challenges for Hypersonic Cruisers", 7th Aerothermodynamics Conference, ATD7-215019, Bruges, Belgium, May 9-12 2011.
4. Steelant, J., Varvill, R., Defoort, S., Hannemann, K., Marini, M., "Achievements Obtained for Sustained Hypersonic Flight within the LAPCAT-II project," 20th AIAA International Space Planes

and Hypersonic Systems and Technologies Conference, Glasgow, Scotland, AIAA-2015-3677, July 5-8 2015.

5. Coleman, C.C., Faruqi, F.A., "On Stability and Control of Hypersonic Vehicles," DSTO-TR-2358, DSTO (Defence Science and Technology Organization) report, 2009.
6. Langener T., Steelant J., P. Roncioni, Natale P. and Marini M., 'Preliminary Performance Analysis of the LAPCAT-MR2 by means of Nose-to-Tail Computations', 18th AIAA International Space Planes and Hypersonic Systems and Technologies Conference, September 24-28, 2012, Tours, France, AIAA-2012-5872. DOI 10.2514/6.2012-5872
7. Steelant J. and Langener T., 'The LAPCAT-MR2 Hypersonic Cruiser Concept', ICAS-2014-0428, 29th Congress of the International Council of the Aeronautical Sciences, St. Petersburg, September 7-12, 2014.
8. Langener, T., Erb, S., Steelant, J., "Trajectory Simulation and Optimization of the LAPCAT MR2 Hypersonic Cruiser Concept," ICAS 2014-0428, 29th Congress of the International Council of the Aeronautical Sciences, St. Petersburg, Russia, Sept. 7-12 2014.
9. Meerts, C., Steelant, J., "Air Intake Design for the Acceleration Propulsion Unit of the LAPCAT-MR2 Hypersonic Aircraft," 5th European Conference for Aeronautics and Space Sciences (EUCASS), Munich, Germany, July 1-5 2013.
10. Gruhn, P., Gülhan, A., "Experimental investigation of a 3d stream-traced air-inlet for a scramjet engine," SP2014-2971058, 3AF Space Propulsion 2014, Cologne, Germany, May 19-22 2014.
11. Pezzella, G.; Marini, M.; Cicala, M.; Vitale, A.; Langener, T.; Steelant, J.; "Aerodynamic Characterization of HEXAFLY Scramjet Propelled vehicle", AIAA-2014-2844, 32nd AIAA Applied Aerodynamics Conference, AIAA Aviation and aeronautics Forum and exposition 2014, Atlanta, GE, USA, June 16-20 2014.
12. Steelant, J.; Langener, T.; Di Matteo, F.; Hannemann, K.; Riehmer, J.; Kuhn, M.; Dittert, C., Scheuerpflug, F.; Jung, W.; Marini, M.; Pezzella, G., Cicala, M.; Serre, L.; "Conceptual Design of the High-Speed Propelled Experimental Flight Test Vehicle HEXAFLY", AIAA-2015-3539, 20th AIAA International Space Planes and Hypersonic Systems and Technologies Conference, Glasgow, Scotland, 6-9 July 2015